

Direct Observation of Ag Filamentary Paths in Organic Resistive Memory Devices

Byungjin Cho, Jin-Mun Yun, Sunghoon Song, Yongsung Ji, Dong-Yu Kim,*
and Takhee Lee*

We demonstrate bipolar switching of organic resistive memory devices consisting of Ag/polymer/heavily-doped p-type poly Si junctions in an 8×8 cross-bar array structure. The bistable switching mechanism appears to be related to the formation and rupture of highly conductive paths, as shown by a direct observation of Ag metallic bridges using transmission electron microscopy and energy-dispersive X-ray spectroscopy. Current images of high- and low-conducting states acquired by conducting atomic force microscopy also support this filamentary switching mechanism. The filamentary formation can be described by an electrochemical redox reaction model of Ag. Our results may also be applied to other kinds of organic materials presenting similar switching properties, contributing to the optimization of device scaling or memory performance improvement.

1. Introduction

Organic resistive memory devices, based on a resistance change modulated by an electrical stimulus, have been identified as one of the potential candidates for next-generation information storage.^[1–8] The reading of resistance states in resistive switching devices is non-destructive, and no electrical power is needed to maintain the resistance within a given state, which is described by non-volatile memory functionality.^[1–3] In addition, the technical advantages of the fabrication process, such as simplicity,^[9] flexibility,^[10,11] and stackability,^[12,13] would enable the potential availability for low-cost memory applications. In this context, much effort has been devoted to developing functional organic materials,^[14,15] optimizing device structures,^[16] and improving memory performance.^[17,18] However, the switching mechanism is still a controversial issue.

Various switching mechanisms, including conformational change,^[7] charge transfer,^[19] charge trapping,^[20] and filament formation mechanisms,^[21] have been proposed. Particularly, the electrical bistability phenomena in many organic materials have been supported by the filamentary switching mechanism.^[21–23] In general, if the current flow in a low-resistance state occurs in a small fraction of the device area, the phenomenon is usually called filamentary conduction.^[23] Although it is difficult to

elucidate the nature of the localized conductive paths, two kinds of filamentary conduction have been suggested. One kind is associated with carbon-rich filaments formed by the local degradation of organic films,^[24,25] and the other kind is associated with metallic bridges resulting from the migration of electrodes.^[26,27] The latter has been considered to be more common than the former. Several analysis methods have been widely employed to confirm the filamentary switching effect.^[21,22] For example, temperature-variable current-voltage measurements have been found to represent the metallic property of the low-resistance state, i.e., linearly increasing resistance with increasing temperature in

the case of conduction through metal elements.^[22] Elemental depth profiles using X-ray photoelectron spectroscopy or secondary ion mass spectroscopy have verified the presence of top metal elements diffusing into the organic matrix.^[21] Area independence of the low-resistance state is also indirect evidence of localized conduction through a small area.^[28] However, it has been challenging to clearly understand the shape of the filamentary paths and their elemental composition. To attain such information would require advanced tools for atomic-scale analysis, e.g., high-resolution transmission electron microscopy (TEM) and elemental analysis. Nevertheless, conductive paths commonly occur in very limited areas of the device junction so that TEM samples prepared by the focused ion beam technique may often not include the area of interest corresponding to the filamentary paths. The amount of metal atoms diffused into the organic layer can often be very small, which makes it difficult to distinguish distinct image features from the polymer. Many previous studies regarding resistive switching mechanisms have failed to achieve direct imaging of conductive filamentary paths connecting the electrodes due to these limitations.

Here, we successfully demonstrate that the reversible resistive switching of a Ag/polymer/heavily-doped p-type poly Si structure is associated with the formation and rupture of highly conductive paths, which is clearly validated by the direct observation of Ag metallic bridges within the organic material by TEM and energy-dispersive X-ray spectroscopy (EDX). Furthermore, conducting atomic force microscopy (CAFM) experiments were used to visualize the localized current distribution through the highly conductive paths. We also suggest that an electrochemical redox reaction model of the top electrode (Ag) can explain the formation and rupture of Ag metallic bridges causing the switching phenomena.

B. Cho, J.-M. Yun, S. Song, Y. Ji, Prof. D.-Y. Kim, Prof. T. Lee
School of Materials Science and Engineering
Gwangju Institute of Science and Technology (GIST)
1 Oryong-Dong, Buk-Gu, Gwangju 500-712, Korea
E-mail: kimdy@gist.ac.kr; tlee@gist.ac.kr

DOI: 10.1002/adfm.201101210

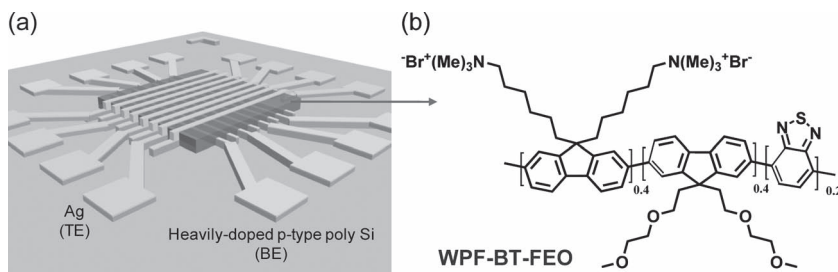


Figure 1. a) A schematic of the Ag/WPF-BT-FEO/heavily-doped p-type poly Si organic resistive memory device with an 8 × 8 array structure. b) The chemical structure of the WPF-BT-FEO polymer.

2. Results and Discussion

An organic resistive memory device consisting of Ag/poly[(9,9-bis(6'-N,N,N-trimethylammonium hexyl)-2,7-fluorene)-co-(9,9-bis(2-(2-methoxyethoxy)ethyl)-fluorene)-co-(2,1,3-benzothiadiazole)] dibromide (denoted as WPF-BT-FEO)/heavily-doped p-type poly Si layers is illustrated in Figure 1a. The memory device contains 8 × 8 cells, in which the junction area of a cell is 100 μm × 100 μm. The chemical structure of the WPF-BT-FEO polymer used as an active layer in the organic memory device is schematically displayed in Figure 1b. The details of material preparation and device fabrication are provided in the Experimental section.

Figure 2a shows the representative current-voltage (*I*-*V*) characteristics of the organic memory devices. A voltage was applied to the Ag top electrode while the heavily-doped p-type poly Si bottom electrode was grounded. When a positive voltage from 0 to 5 V was applied to the Ag top electrode, the current gradually increased in the low bias region, and then an abrupt increase in current was observed near the threshold voltage, indicating a set process from a high-resistance state (HRS) to a low-resistance state (LRS) (first curve). The threshold voltage was defined as the point in the conductance-voltage curve (first derivative of *I*-*V* curve) where the conductance value abruptly increases and in more detail, the point where over 10-fold increase in conductance value occurs (see Figure S5 in the Supporting Information). To prevent electrical breakdown of the device, the compliance current was set to 0.1 mA. Even after the set process, the LRS was well maintained during the voltage sweep from 5 to 0 V (second curve). When a negative voltage was applied to the device, the device current rapidly decreased, which is associated with a reset process from the LRS to the HRS (third curve). After this reset process, the HRS remained (fourth curve). Consequently, the different voltage polarity demonstrated reversible resistive switching in our device (i.e., positive and negative voltages are applied for the set and reset processes, respectively), which is called bipolar memory. A high ON/OFF ratio of over 10⁴ was observed at the read voltage region, as shown in Figure 2b. The memory margin was large enough to distinguish each resistance state in our memory devices.

The switching mechanism in organic resistive memory devices has been the subject of

much debate. Although electrical bistability of many organic materials has been reported, the proposed switching mechanisms are still not clear. Furthermore, bistable switching events appear to be caused by factors other than the organic material itself because the switching characteristics strongly depend on interface states and the kind of electrodes used.^[29,30] Therefore, it is very challenging to thoroughly understand the underlying physics of the resistive switching phenomena and to validate the nature of the switching events.

TEM is a powerful analysis tool for identifying what changes occur within the organic materials according to the resistance states. Figure 3a-c show a series of cross-sectional TEM images of memory cells in different resistance states: the HRS (pristine), the LRS (after the set process), and the HRS (after the reset process). To identify the elements within the organic material, EDX was also carried out for the same TEM specimens, as shown in Figures 3d-f. First, Figure 3a shows a cross-sectional TEM image of the memory cell in the pristine HRS. Shallow penetration (~10 nm) of Ag metal into the organic layer was found, which is due to thermal diffusion during the Ag metal deposition. However, we did not observe any completely connected Ag bridges between the top and bottom electrodes. This is clearly shown in Figure 3c, in which the EDX profile for the Ag element was obtained across a line indicated in Figure 3a. The results of Figure 3a and d explain why the memory cell initially showed the electrically insulating property, i.e., the HRS.

However, one can clearly see that the memory cell that had switched from the HRS to the LRS had irregularly shaped electrical pathways (dark region in the organic layer), as shown in Figure 3b. The intensity of Ag along the Ag/WPF-BT-FEO/heavily-doped p-type single crystalline Si layers was observed. In particular, a line profile of the intensity of Ag along the dark region was attained by EDX measurement, as shown in Figure 3e. It was verified that the pathway is mainly composed of Ag and that the Ag extends into the heavily-doped p-type single crystalline Si bottom electrode. The results of Figures 3b and 3e imply that the Ag has not only thoroughly penetrated through the organic layer but has also connected the two electrodes completely. As a consequence, the LRS is obtained due to the connected metallic pathways between the two electrodes.

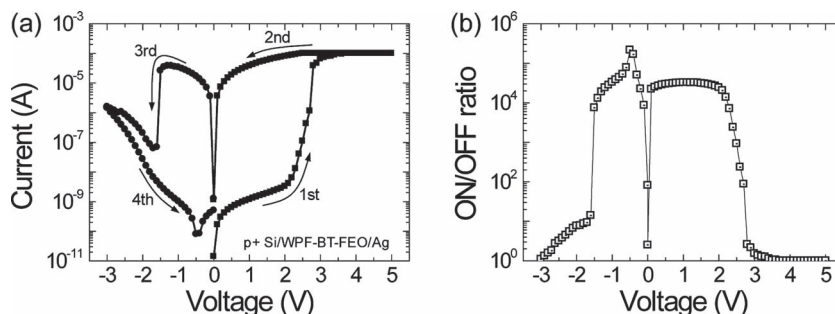


Figure 2. a) Representative *I*-*V* characteristics of the Ag/WPF-BT-FEO/heavily-doped p-type poly Si devices showing the bipolar switching property. b) The ON/OFF ratio as a function of voltage.

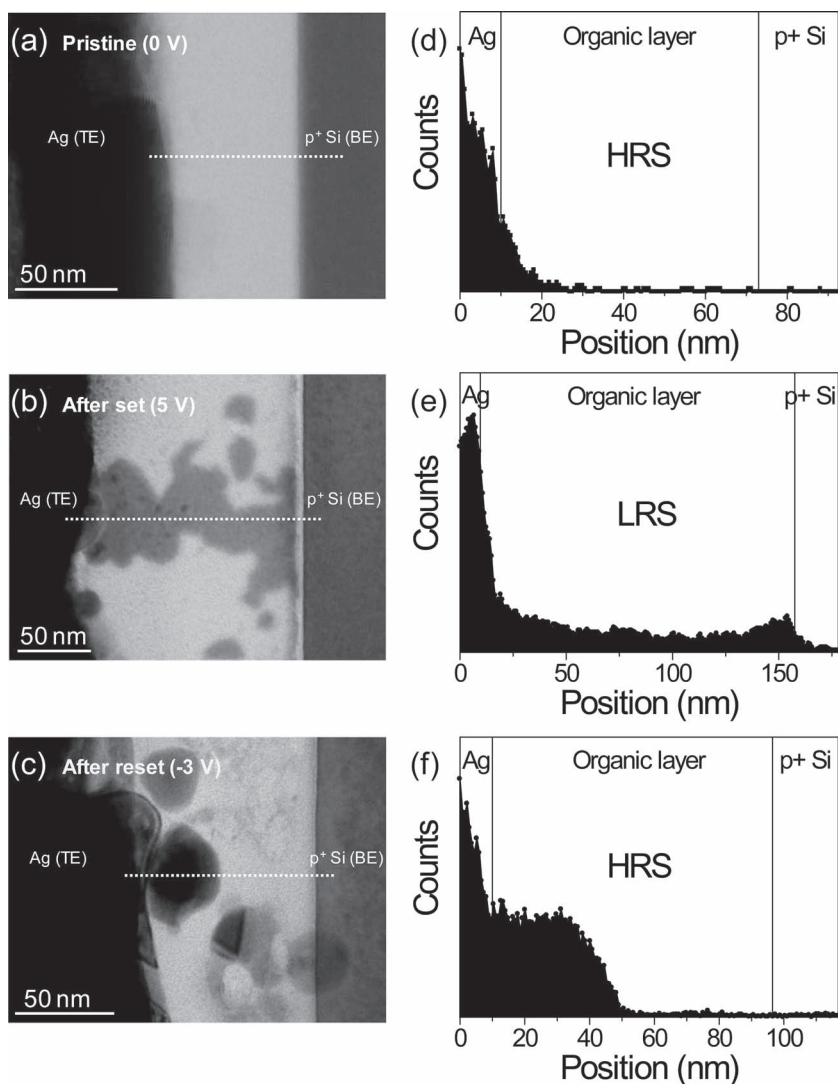


Figure 3. a–c) Cross-sectional TEM images of memory cells in different resistance states. d–f) EDX analysis for Ag element profiles along the dotted lines marked in (a)–(c). a) Cross-sectional TEM image and d) Ag element profile of the Ag/WPF-BT-FEO/heavily-doped p-type single crystalline Si memory cell in the pristine HRS when no voltage is applied to the device. b) Cross-sectional TEM image and e) Ag element profile of the Ag/WPF-BT-FEO/heavily-doped p-type single crystalline Si memory cell programmed into the LRS after applying the set voltage (5 V). The dark regions within the organic layer extending to the heavily-doped p-type single crystalline Si include Ag, forming metallic bridges between the top and bottom electrodes. c) Cross-sectional TEM image and f) Ag element profile of the Ag/WPF-BT-FEO/heavily-doped p-type single crystalline Si memory cell returning to the HRS after applying the reset voltage (–3 V). A few Ag islands exist independently within the organic layer, but they do not connect the two electrodes.

Analyses for other regions of the TEM specimen also yielded similar results.

A cross-sectional TEM image of the memory cell that had been returned to the HRS by a reset voltage of –3 V was also captured (Figure 3c). There are a few regions within the organic layer that exist randomly and independently, without any complete connections. Ag below the top electrode is clearly detected, but the Ag does not extend to the heavily-doped p-type single crystalline Si bottom electrode, as shown in Figure 3f. That is, we did not observe any completely connected metallic

bridges between the top and bottom electrodes, demonstrating that the HRS is caused by the rupture of the Ag metallic pathways. Therefore, according to these TEM and EDX observations, the bistable switching phenomena in our devices should be associated with the formation and rupture of filamentary paths mainly consisting of Ag.

To further investigate the switching mechanism, we examined the current images of the LRS and the HRS for Ag (10 nm)/WPF-BT-FEO/heavily-doped p-type single crystalline Si layers using conducting atomic force microscopy (CAFM), as shown in Figure 4. Here, a thin Ag film (10 nm) was used for the purpose of reducing the contact resistance between the CAFM tip and the organic sample. We used a conductive cantilever coated with Ag as a movable top electrode. The AFM tip was first scanned over an area of 500 nm × 500 nm under a tip bias of 5 V with respect to heavily-doped p-type single crystalline Si, and then a current image of the LRS was obtained under a –1 V tip bias (Figure 4b). Similarly, a current image of the HRS was obtained at a –1 V tip bias after the CAFM tip was scanned under a –3 V tip bias (Figure 4a). As shown in Figure 4a, the current distribution of the HRS remained uniform, with a low current level over the whole scanned region. In contrast, the current of the LRS (Figure 4b) was observed to be locally distributed over a few limited spots of the scanned region, and its peak current level was 250 times higher than that of the HRS. This observation implies that the highly conductive paths of the LRS in the memory devices do not occur uniformly over the junction area. Although the sizes of the localized conductive paths obtained in the CAFM experiment are not perfectly consistent with the results from the TEM images (Figure 3), it is evident that the LRS is caused by locally distributed metallic filamentary paths within the organic layer consisting of Ag.

By combining the bipolar switching effect and the existence of metallic Ag bridges, now we can suggest a clearer switching model describing how Ag bridges form and rupture within the organic layer. The model is based on a creation-and-rupture process of redox-controlled metal bridges.^[21,31–34] When a positive voltage is applied to the Ag top electrode, oxidation occurs on this electrochemically active material, described by $\text{Ag} \rightarrow \text{Ag}^+ + \text{e}^-$. The mobile Ag^+ cations diffuse toward the heavily-doped p-type single crystalline Si bottom electrode through the organic layer and are reduced there by electrons flowing from the bottom electrode, i.e., $\text{Ag}^+ + \text{e}^- \rightarrow \text{Ag}$. With the successive precipitation of Ag, the metal starts to grow at the bottom electrode, then reaches the Ag top electrode, and finally forms Ag

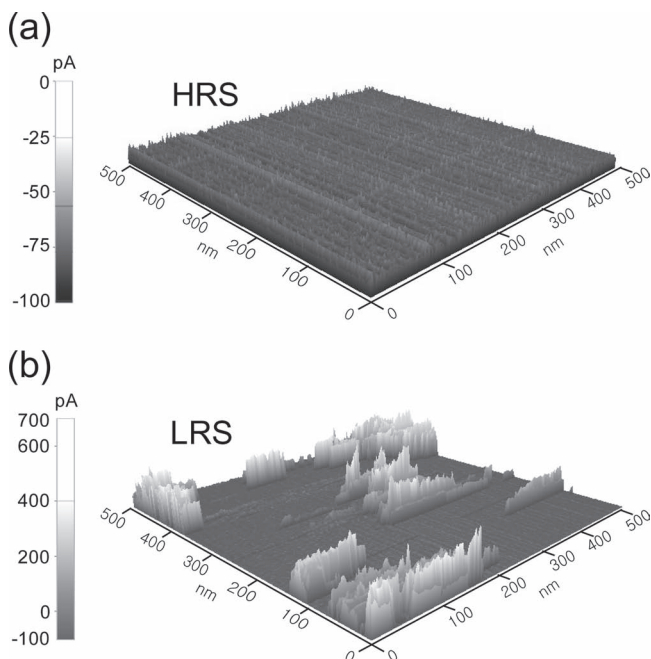


Figure 4. Current images of the a) HRS and b) LRS in a WPF-BT-FEO organic resistive memory device obtained by CAFM measurements.

metallic bridges between the two electrodes. When the voltage polarity is reversed, an electrochemical dissolution takes place somewhere along the bridge, resetting the system into the HRS. Although the exact point at which the rupture takes place is still unclear, it is reasonable that rupture would occur at the weakest part of the bridge.^[34]

We calculated and summarized a few important parameters which are involved in electrochemical process of Ag atoms (see Table S2 in the Supporting information). From TEM image data of LRS cell, the total volume of electrodeposited Ag atoms in junction area of $100\ \mu\text{m} \times 100\ \mu\text{m}$ was roughly estimated to be about $3.5 \times 10^{-17}\ \text{m}^3$. It implies that 2×10^{12} Ag atoms were deliberated from top electrodes and thus Ag atoms of $3.6 \times 10^{-10}\ \text{g}$ were electrodeposited within the polymer layer. According to the Faraday's law, the amount of charge flowing through the electrodeposited Ag was calculated to be $3.2 \times 10^{-7}\ \text{C}$, which was even smaller than total amount of charge ($10^{-4}\ \text{C}$) flowing through the junction area (see Figure 2a). From these results, it was found that a very small fraction of total current flowing through the junction is involved with the electrochemical reaction of Ag bridges connecting two electrodes. The careful control of the density and strength of the metallic bridges would be essential for modulating various memory parameters such as HRS, LRS, ON/OFF ratio, endurance, and retention properties.

To investigate the role of polymer layer in resistive switching, we fabricated and characterized devices made with other polymer materials such as spin-on glass (SOG) and poly(3-hexylthiophene) (P3HT) (see Figure S6 in the Supporting Information). We observed that the insulating polymers of SOG exhibited only the set process without reset process (Figure S6a) while the semiconducting polymer of P3HT exhibited the bipolar switching behavior (Figure S6b). However, OFF current

of the P3HT based memory device was relatively higher than that for WPF-BT-FEO devices, producing lower ON/OFF ratio, indicating that most of charges in pristine HRS pass through the whole semiconducting polymer layer. From all these results, kind of the active polymer is also greatly important for reversible switching phenomenon to the acceptable level.

Regarding the role of Br^- anions in resistive switching, we attempted to fabricate and characterize devices made with three polyfluorene derivative polymers, all of which contain Br^- anions: poly[(9,9-bis(60-(N,N,N-trimethylammonium) hexyl)-2,7-fluorene)-alt-1,4-xylene] dibromide (denoted as WPXF), poly[(9,9-bis(60-(N,N,N-trimethylammonium) hexyl)-2,7-fluorene)-alt-1,4-(2,5-dimethoxybenzene)] dibromide (denoted as WPmXF), and poly[(9,9-bis(60-(N,N,N-trimethylammonium) hexyl)-2,7-fluorene)-alt-(9,9-bis(2-(2-methoxyethoxy)ethyl)-fluorene)] dibromide (denoted as WPF-oxy-F). *I-V* results of the devices with the polyfluorene derivatives are summarized (see Figure S7 in the Supporting Information). Interestingly, we observed switching behaviors only in the case of WPF-oxy-F polymer (Figure S7c) while there was no switching behavior in WPXF (Figure S7a) and WPmXF (Figure S7b) based devices. The effect of the Br^- anions on the resistive switching was negligible. Br^- anions simply play a role as a water-soluble moiety to increase solubility between polymer and solvent. Rather, ethylene oxide group in WPF-oxy-F seems to play more critical role for the resistive switching in the polyfluorene derivative polymers because only the WPF-oxy-F polymer with the ethylene oxide group showed the bipolar switching. WPF-BT-FEO polymer used in this work also has the ethylene oxide group which contributes to the reversible resistive switching on the basis of the filamentary mechanism. The side chains of the ethylene oxide act as strong metal coordinating sites, which would be more necessary for metal filament formation. Similarly, other groups have previously reported that the polymers with strongly coordinating heteroatom (S or N) can support the reproducible filament formation behavior.^[22]

To check the switching speed of WPF-BT-FEO based memory device, we measured transient response time under the pulse mode (see Figure S8 in the Supporting Information). We found that even the pulse voltage with a short pulse width of $100\ \mu\text{s}$ could program the memory devices. More specifically, the transient response time of WPF-BT-FEO based memory device was observed to be less than $1\ \mu\text{s}$, indicating the feasibility of ultra high speed memory applications. Indeed, the switching speed of WPF-BT-FEO polymer with the benzothiadiazole (BT) group was much faster than that ($\sim 2\ \text{ms}$) of WPF-oxy-F without the BT group presented in the previous paper.^[35] The choice of WPF-BT-FEO polymer in this study can be certainly advantageous in this aspect. Although the cause of the increased switching speed in WPF-BT-FEO based device is not thoroughly understood, we believe that it might be due to the increase of the mobility of the Ag atoms or cations involved with the electrochemical reaction and/or the increase of the metal coordinating sites by introduction of the BT units. Based on these valid experimental evidences, we concluded that the metal coordinating sites such as ethylene oxide and heteroatom in the semiconducting polymers contribute to the increase in electrochemical reaction speed as well as the reproducible filament formation.

We noted that humidity can sometimes influence resistive switching involved with electrochemical process.^[36] To investigate the effect of humidity on electrical property of WPF-BT-FEO organic resistive memory device, we compared I - V curves measured under each different relative humidity condition of 19% and 40% (see Figure S9 in the Supporting Information). Almost the same I - V characteristics were obtained in our memory devices regardless of the humidity content. Threshold voltages necessary for set and reset process were also nearly similar. From this result, we think that humidity effect on resistive switching properties of our memory devices is negligible. In contrast, Knorr et al.^[36] reported that the increase of humidity in Cu/P3HT/Au junctions caused electrical hysteresis phenomenon, which was explained by field-absorbed water induced electrochemical process. The electrochemical process involved sequential chemical reactions as following: diffusion of copper ions from the Cu electrode, P3HT decomposition, and the formation of copper sulfide crystals by the reaction between released sulfur and copper ions which was considered to be important precursors to metal filament formation. We expect that somewhat different experimental results between our and Knorr's work might result from the difference in kind of polymer, polymer thickness, and kind of electrodes.

For a memory device, it is important to investigate the statistical distribution of essential memory parameters, such as the resistance values of each state and the threshold voltages in cross-bar array memory devices. Figure 5a shows the cumulative probability data for the HRS and LRS of 64 memory cells with the 8×8 array structure. The resistance values were densely distributed, indicating a good cell-to-cell uniformity. More importantly, the distribution of the HRS was well separated from that of the LRS, which provided a good margin of the ON and OFF states in the memory devices. Nevertheless, cross-talk problem can often occur in the cross-bar structure containing only memory elements.^[5] To resolve this issue, memory devices with self-rectifying property^[37] or additional switching components such as transistor or diode^[5,38,39] should be developed. Our next study will focus on such a research topic.

We also extracted threshold voltages (transition voltage from the HRS to the LRS) from I - V curves of 64 memory cells. The inset of Figure 5b shows a histogram of the threshold voltages, which are distributed in a narrow range from 1.5 to 2.5 V. A small voltage range is required to minimize programming failure during the set process. To evaluate the information storage ability, we also carried out a retention test for each resistance state, as shown in Figure 5b. Each state presented stable retention characteristics without any electrical degradation up to 10^4 sec. In addition, a high ON/OFF ratio of $\sim 10^4$ was well maintained during the retention test. To check the spread evolving with increasing sweep cycles, we also tested endurance characteristics using repetitive sweep mode (0 to 5 V for set process and 0 to -5 V for reset process). Although scattering data in both HRS and LRS were occasionally observed, the HRS values were fairly separated from the LRS for more than 1000

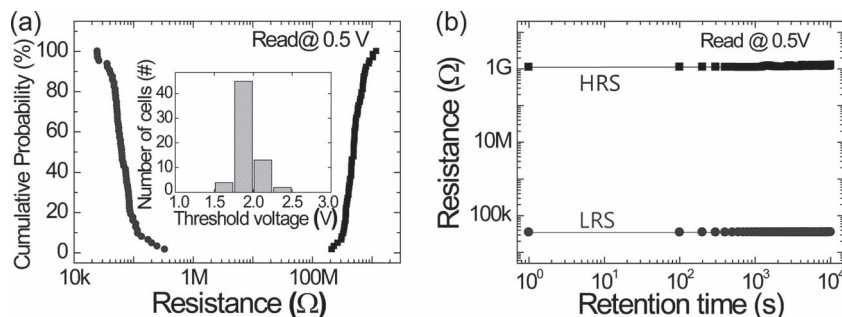


Figure 5. a) The cumulative probability data of each resistance state for the Ag/WPF-BT-FEO/heavily-doped p-type poly Si organic resistive memory devices in 8×8 array cells. The inset shows the threshold voltage distribution. b) The retention time of the Ag/WPF-BT-FEO/heavily-doped p-type poly Si organic resistive memory devices.

cycles (see Figure S10 in the Supporting Information). These high performance characteristics are essential for more practical memory device applications.

3. Conclusions

In summary, we have experimentally shown that the bipolar switching of WPF-BT-FEO based organic memory devices is associated with the formation and rupture of Ag metallic bridges connecting two electrodes, which is supported by TEM and EDX analyses. CAFM measurements were also used to visualize the localized conductive paths of low-resistance states. The electrochemical redox reaction model of Ag is suggested to describe how the metallic bridges are formed and broken within the organic layer. Understanding the switching mechanism in organic resistive memory devices can lead to improvements in memory performance and the optimization of device scaling.

4. Experimental Section

Bottom Electrodes: Organic resistive memory devices were fabricated on a heavily-doped p-type poly Si layer on SiO_2/Si wafer. The thickness of the heavily-doped p-type poly Si and SiO_2 film, used as bottom electrodes and insulating layer, was measured to be approximately 200 and 300 nm, respectively. The Si wafer was cleaned using an ultrasonic system with acetone, methanol, and DI water. To make devices in 8×8 cross-bar array cells, 8 poly-Si lines of 100- μm in width were patterned as bottom electrodes using conventional optical lithography and the sequential reactive ion etching process (rf power = 50 W, pressure = 50 mTorr, SF_6 gas = 40 SCCM (SCCM denotes cubic centimeters per minute at STP), and etching time = 100 sec). The Si wafer was treated via a diluted HF-last process to remove the native oxide layer.

Organic Active Layer: A polyfluorene derivative, poly[(9,9-bis(6'-(N,N,N-trimethylammonium) hexyl)-2,7-fluorene)-co-(9,9-bis(2-(2-methoxyethoxy)ethyl)-fluorene)-co-(2,1,3-benzothiadiazole)] dibromide (denoted as WPF-BT-FEO), was synthesized by a palladium-catalyzed Suzuki coupling reaction method (see Figure S1 in the Supporting Information) and then was characterized by UV-vis spectra, cyclic voltammetry (see Figure S2 in the Supporting Information), thermogravimetric analysis, and differential scanning calorimetry (see Figure S3 in the Supporting Information). Highest occupied molecular orbital and bandgap of WPF-BT-FEO were calculated from the onset voltage in cyclic voltammetry and the absorption onset in UV-vis spectra, respectively. The resulting highest occupied molecular orbital,

lowest unoccupied molecular orbital, and bandgap of WPF-BT-FEO were summarized (see Table S1 of the Supporting Information). WPF-BT-FEO was first dissolved in methanol at a concentration of 5 mg/mL and was then spin-coated onto the patterned bottom electrodes at 1000 rpm for 40 sec. To improve the film uniformity and to eliminate the solvent from the film, a post-baking step was performed at 150 °C for 20 min on a hot plate in a nitrogen-filled glove box.

Top Electrodes: A shadow mask with 100- μm line patterns was vertically aligned with the bottom electrode lines, thus making a junction area of 100 $\mu\text{m} \times 100 \mu\text{m}$. Consequently, a 50-nm-thick Ag layer (with a deposition rate of 3 Å/sec) was deposited as the top electrodes using an e-beam evaporator at a pressure of $\sim 10^{-6}$ Torr. The device structure of Ag/WPF-BT-FEO/heavily-doped p-type poly Si was finally completed (see Figure S4 in the Supporting Information). Room temperature *I*-*V* measurements of the fabricated devices were performed under an ambient atmosphere using a semiconductor parameter analyzer (Agilent 4155C).

Transmission Electron Microscopy (TEM) and energy-dispersive X-ray spectroscopy (EDX) analysis: Samples consisting of the Ag (50 nm)/WPF-BT-FEO/heavily-doped p-type single crystalline Si structure were prepared for TEM analysis. The thickness of the heavily-doped p-type single crystalline Si, used as bottom electrodes and substrate, was approximately 680 μm . The samples had a few unit cells with a junction area of 300 $\mu\text{m} \times 300 \mu\text{m}$. After applying different voltages (0, 5, and -3 V) to each memory cell, cross-sectional TEM images and EDX line profiles were obtained from three TEM specimens prepared by focused ion beam milling.

Conducting Atomic Force Microscopy (CAFM) measurement: Samples for CAFM measurements were fabricated with the Ag (10 nm)/WPF-BT-FEO/heavily-doped p-type single crystalline Si structure. A thin Ag film was added to the organic layer to reduce the contact resistance between the conductive cantilever and the organic layer. A conductive cantilever tip coated with Ag (10 nm) was used as a movable top electrode. Current images of the high and low-resistance states for the WPF-BT-FEO-based device were obtained using an AFM (Park Systems XE-100).

Supporting Information

Supporting Information is available from the Wiley Online Library or from the author.

Acknowledgements

B.C. and J.-M.Y. contributed equally to this work. This work was supported by the National Research Laboratory program, a National Core Research Center grant, the World Class University program of the Korean Ministry of Education, Science and Technology, the Program for Integrated Molecular Systems/GIST, and the IT R&D program of MKE/KEIT.

Received: May 27, 2011

Published online: August 24, 2011

- [1] Y. Yang, J. Ouyang, L. Ma, R. J. H. Tseng, C. W. Chu, *Adv. Funct. Mat.* **2006**, 16, 1001.
- [2] J. C. Scott, L. D. Bozano, *Adv. Mater.* **2007**, 19, 1452.
- [3] Q.-D. Ling, D.-J. Liaw, C. Zhu, D. S.-H. Chan, E.-T. Kang, K.-G. Neoh, *Prog. Polym. Sci.* **2008**, 33, 917.
- [4] L. D. Bozano, B. W. Kean, M. Beinhoff, K. R. Carter, P. M. Rice, J. C. Scott, *Adv. Funct. Mat.* **2005**, 15, 1933.
- [5] B. Cho, T.-W. Kim, S. Song, Y. Ji, M. Jo, H. Hwang, G.-Y. Jung, T. Lee, *Adv. Mater.* **2010**, 22, 1228.
- [6] B. Cho, S. Song, Y. Ji, T. Lee, *Appl. Phys. Lett.* **2010**, 97, 063305.
- [7] Z. J. Donhauser, B. A. Mantooth, K. F. Kelly, L. A. Bumm, J. D. Monnell, J. J. Stapleton, D. W. Price, A. M. Rawlett, D. L. Allara, J. M. Tour, P. S. Weiss, *Science* **2001**, 292, 2303.
- [8] S. Möller, C. Perlov, W. Jackson, C. Taussig, S. R. Forrest, *Nature* **2003**, 426, 166.
- [9] K. Asadi, M. Li, N. Stingelin, P. W. M. Blom, D. M. de Leeuw, *Appl. Phys. Lett.* **2010**, 97, 193308.
- [10] Y. Ji, B. Cho, S. Song, T.-W. Kim, M. Choe, Y. H. Kahng, T. Lee, *Adv. Mater.* **2010**, 22, 3071.
- [11] L. Li, Q.-D. Ling, S.-L. Lim, Y.-P. Tan, C. Zhu, D. S. H. Chan, E.-T. Kang, K.-G. Neoh, *Org. Electron.* **2007**, 8, 401.
- [12] S. Song, B. Cho, T.-W. Kim, Y. Ji, M. Jo, G. Wang, M. Choe, Y. H. Kahng, H. Hwang, T. Lee, *Adv. Mater.* **2010**, 22, 5048.
- [13] J.-G. Park, W.-S. Nam, S.-H. Seo, Y.-G. Kim, Y.-H. Oh, G.-S. Lee, U.-G. Paik, *Nano Lett.* **2009**, 9, 1713.
- [14] X.-D. Zhuang, Y. Chen, G. Liu, B. Zhang, K.-G. Neoh, E.-T. Kang, C.-X. Zhu, Y.-X. Li, L.-J. Niu, *Adv. Funct. Mat.* **2010**, 20, 2916.
- [15] E. Y. H. Teo, Q. D. Ling, Y. Song, Y. P. Tan, W. Wang, E. T. Kang, D. S. H. Chan, C. Zhu, *Org. Electron.* **2006**, 7, 173.
- [16] B. Lei, W. L. Kwan, Y. Shao, Y. Yang, *Org. Electron.* **2009**, 10, 1048.
- [17] T. Kondo, S. M. Lee, M. Malicki, B. Domercq, S. R. Marder, B. Kippelen, *Adv. Funct. Mat.* **2008**, 18, 1112.
- [18] J. Chen, D. Ma, *J. Appl. Phys.* **2006**, 100, 034512.
- [19] Y. Song, Q. D. Ling, S. L. Lim, E. Y. H. Teo, Y. P. Tan, L. Li, E. T. Kang, D. S. H. Chan, C. Zhu, *IEEE Electron Device Lett.* **2007**, 28, 107.
- [20] L. D. Bozano, B. W. Kean, V. R. Deline, J. R. Salem, J. C. Scott, *Appl. Phys. Lett.* **2004**, 84, 607.
- [21] W.-J. Joo, T.-L. Choi, K.-H. Lee, Y. Chung, *J. Phys. Chem. B* **2007**, 111, 7756.
- [22] W.-J. Joo, T.-L. Choi, J. Lee, S. K. Lee, M.-S. Jung, N. Kim, J. M. Kim, *J. Phys. Chem. B* **2006**, 110, 23812.
- [23] T.-W. Kim, S.-H. Oh, H. Choi, G. Wang, H. Hwang, D.-Y. Kim, T. Lee, *Appl. Phys. Lett.* **2008**, 92, 253308.
- [24] L. F. Pender, R. J. Fleming, *J. Appl. Phys.* **1975**, 46, 3426.
- [25] Y. Segui, B. Ai, H. Carchano, *J. Appl. Phys.* **1976**, 47, 140.
- [26] G. Dearnaley, D. V. Morgan, A. M. Stoneham, *J. Non-Cryst. Solids* **1970**, 4, 593.
- [27] W. Hwang, K. C. Kao, *J. Chem. Phys.* **1974**, 60, 3845.
- [28] T.-W. Kim, H. Choi, S.-H. Oh, M. Jo, G. Wang, B. Cho, D.-Y. Kim, H. Hwang, T. Lee, *Nanotechnology* **2009**, 20, 025201.
- [29] B. Mukherjee, A. J. Pal, *Org. Electron.* **2006**, 7, 249.
- [30] Y. Li, D. Qiu, L. Cao, C. Shao, L. Pan, L. Pu, J. Xu, Y. Shi, *Appl. Phys. Lett.* **2010**, 96, 133303.
- [31] S. Ssenyange, H. Yan, R. L. McCreery, *Langmuir* **2006**, 22, 10689.
- [32] Y. C. Yang, F. Pan, Q. Liu, M. Liu, F. Zeng, *Nano Lett.* **2009**, 9, 1636.
- [33] R. Waser, R. Dittmann, G. Staikov, K. Szot, *Adv. Mater.* **2009**, 21, 2632.
- [34] X. Guo, C. Schindler, S. Menzel, R. Waser, *Appl. Phys. Lett.* **2007**, 91, 133513.
- [35] T.-W. Kim, S.-H. Oh, J. Lee, H. Choi, G. Wang, J. Park, D.-Y. Kim, H. Hwang, T. Lee, *Org. Electron.* **2010**, 11, 109.
- [36] N. Knorr, R. Wirtz, S. Rosselli, G. Nelles, *J. Phys. Chem. C* **2010**, 114, 15791.
- [37] K. Asadi, D. M. de Leeuw, B. de Boer, P. W. M. Blom, *Nat. Mater.* **2008**, 7, 547.
- [38] M. J. Lee, Y. Park, D. S. Suh, E. H. Lee, S. Seo, D. C. Kim, R. Jung, B. S. Kang, S. E. Ahn, C. B. Lee, D. H. Seo, Y. K. Cha, I. K. Yoo, J. S. Kim, B. H. Park, *Adv. Mater.* **2007**, 19, 3919.
- [39] T.-W. Kim, H. Choi, S.-H. Oh, G. Wang, D.-Y. Kim, H. Hwang, T. Lee, *Adv. Mater.* **2009**, 21, 2497.